

Investigation of acoustic properties of rubber diaphragm

Ziyu Wang

Applied Mechanics Lab, Department of Engineering Mechanics, Tsinghua University, Beijing 100084, China; wangziyu18@tsinghua.org.cn

CITATION

Wang Z. Investigation of acoustic properties of rubber diaphragm. *Sound & Vibration*. 2025; 59(2): 2707.
<https://doi.org/10.59400/sv2707>

ARTICLE INFO

Received: 2 February 2025
Accepted: 11 March 2025
Available online: 18 March 2025

COPYRIGHT



Copyright © 2025 by author(s).
Sound & Vibration is published by Academic Publishing Pte. Ltd. This work is licensed under the Creative Commons Attribution (CC BY) license.
<https://creativecommons.org/licenses/by/4.0/>

Abstract: Large amplitude and high damping play a crucial role in improving sound quality and low-frequency performance of loudspeakers, making it widely applied in electronic devices such as cellphones, tablets, and laptops. However, traditional moving-coil loudspeakers have poor damping performances, and the diaphragm of which is prone to fracture when a large excursion is applied. In this study, a novel ethyl acrylate rubber (AEM) diaphragm was fabricated through solvent casting and thermoforming and assembled to make moving-coil microspeakers (i.e., miniature loudspeakers) with excellent frequency response, amplitude, and damping performances. Meanwhile, the acoustic properties of microspeakers with different diaphragm samples were compared, and the relationships between resonance frequency and elastic modulus in the linear elastic range, the resonance frequency, and mechanical resistance of total-driver losses were revealed and validated by the calculations of mechanical stiffness of driver suspension and mechanical Q-factor of driver. The microspeakers with diaphragm samples “AEM-90-5” fabricated in this study exhibit significant and symmetric excursions; meanwhile, the acoustic properties of microspeakers in the future studies could be optimized by compositions and elastic modulus based on these samples.

Keywords: moving-coil microspeakers; AEM diaphragms; large amplitude; high damping; tuning of acoustic performances

1. Introduction

Miniature loudspeakers, or microspeakers, are electric-acoustic transducers that are widely applied in portable electronic devices. Diaphragms are core sound-stimulated structures in microspeakers and could suspend the voice coil, provide compliance, and effectively separate the front chamber and back chamber of microspeakers. The most-concerned acoustic parameters, including maximum excursion (X_{max}), resonance frequency (F_0), and mechanical resistance of total-driver losses (R_{ms}), are directly influenced by the physical properties of diaphragms.

The first generation of diaphragm was mainly made of paper pulp and its modified materials with the advantages of low cost and easy fabrication. However, paper diaphragms have low tensile strength and durability and are vulnerable to water, thus the sound quality could be affected. The second generation of diaphragm was made of metals and alloys. The metallic diaphragm has higher tensile strength and stiffness and can withstand higher sound pressure; thus, the sound quality is improved; however, the mass of the metallic diaphragm is relatively high, which is harmful for the sensitivity and frequency response range of the microspeaker. The third generation of diaphragm was made of polymers, in that polymers have low density with high stiffness and excellent damping performances; thus, the good sound quality and wide range of frequency response (FR) could be achieved. The most commonly used polymers for diaphragms include poly ether ether ketone (PEEK) and thermoplastic polyester elastomer (TPEE), in which PEEK is an engineering plastic, and TPEE is a

kind of multiblock copolymer built up from short hard segments and long soft segments, providing itself with an unusual combination of thermoplastic and elastomeric behavior [1]. Wang et al. [2] simulated microspeakers with HDPE, PEI, PEEK, and aluminum diaphragms by finite element method (FEM) and obtained a series of FR curves. It was found that for the first mode, the F_0 of HDPE is the lowest due to its lowest elastic modulus, and the F_0 of aluminum is the highest due to its highest elastic modulus. Therefore, the F_0 of a microspeaker is closely related to the elastic modulus or stiffness of the diaphragm. Bae et al. [3] proposed that the materials of diaphragms for a microspeaker should have enough elasticity. In their studies, a PEEK + TPU + PEEK multilayered diaphragm with a thickness of less than 100 μm was designed and thermoformed assisted by ultrasonic energy. Based on mature product information in the market, the receivers with diaphragms made of PEEK usually have an F_0 of approximately 500 Hz with an X_{max} too low to be characterized; the last generation of speakers with diaphragms made of TPEE usually have an F_0 of 750–935 Hz with an X_{max} of 0.3–0.45 mm. Huang et al. [4] fabricated a piezoelectric panel loudspeaker with PEEK for the diaphragm and a piezoelectric panel for the substrate. The as-fabricated loudspeaker has an X_{max} of $\sim 1.5 \mu\text{m}$ and F_0 of 200–400 Hz. Other diaphragm materials have also been investigated in the literature. Lin et al. [5] used self-assembly nanoarchitectonics to fabricate a lightweight hyperbolic paraboloid acoustic diaphragm, which is composed of a polyacrylonitrile (PAN) network combined with graphene oxide (GO) nanolayers. Compared with the commercially available banana pulp diaphragm, the electrospun polyacrylonitrile nanofibers embedded with graphene exhibit long-term stability and durability, and enables the speaker to respond more effectively to acoustic signals, especially at higher frequencies. Bi et al. [6] developed a novel composite diaphragm material by combining the swollen carboxymethyl cellulose microfibers (CMF) with the hot-melt sheath-core fibers (SCF). This bio-based diaphragm material exhibits excellent mechanical properties, including low density, high tensile strength, and high modulus. The fabricated speaker demonstrates higher sensitivity and stable acoustic performance over a wide frequency range. At present, the development trends of diaphragm materials for microspeakers are focused on the following aspects: lightweight, low elastic modulus, high damping performance, durability, and low cost.

The acoustic properties of a microspeaker directly account for its sound quality and are closely related to the structures and properties of the components. The most commonly used testing devices are Soundcheck and Klippel R&D System, in which the FR, electrical impedance (IMP), total harmonic distortion (THD) curves, and Thiele-Small (TS) parameters could be obtained. TS parameters were proposed by Thiele [7,8] and Small [9–12] as fundamental parameters for microspeaker systems in the 1970s and were subsequently tested by Klippel R&D System, also designed by Thiele and Small. As the core component of the vibrating system in the microspeakers, the material nature and the mechanical properties of the diaphragm have a great effect on the acoustic properties of the microspeakers. Hwang et al. [13] prepared headphones based on a graphene oxide paper diaphragm and three types of graphene oxide/epoxy nanocomposite diaphragm. The performance of these headphones based on the sound pressure level (SPL) curves was analyzed by Soundcheck measurement

system, and the compliance of various diaphragms was measured by Klippel LPM laser measurement system. The results showed that a higher damping ratio and lower compliance made the SPL curve of the graphene oxide paper flatter at high frequencies. Sun et al. [14] deposited carbon-like diamond/tungsten coatings on the surface of aluminum-magnesium diaphragms using plasma-enhanced chemical vapor deposition (PECVD). This made the FR curve of the microspeaker smoother, increased the SPL in the high-frequency range, and reduced the THD percentage. They also found that the thinner the coating, the more significant the improvement in the acoustic performance of the microspeaker. Aiming at the phenomenon that the FR performance of the commercially available circular speaker is poor due to the dip of the frequency response (FR) curve in the middle frequency range (near 2500 Hz), Park et al. used polyurethane (PU) as the sound-absorbing material on the reflective surface, which increased the SPL in the middle frequency range by 12.2 dB. Jiang et al. [15] employed the electromagnetic-mechanical-acoustic coupling method and the resonance equation to obtain the SPL and the peak frequency, and designed and fabricated microspeaker samples with different front chamber designs. Meanwhile, based on the acoustic models of the Helmholtz resonator and the tube resonator respectively, they revealed the causes of the mid-frequency peak and the high-frequency peak on the FR curve. Aiming at the phenomenon that the FR performance of the commercially available circular speaker is poor due to the dip of the frequency response (FR) curve in the middle frequency range (near 2500 Hz), Park et al. [16] used polyurethane (PU) as the sound-absorbing material on the reflective surface, which increased the SPL in the middle frequency range by 12.2 dB. Other researches focus on piezoelectric loudspeakers, which have higher SPL and lower amplitudes compared to moving-coil loudspeakers. Ma et al. [17] proposed a novel piezoelectric micro-electromechanical systems (MEMS) speaker with a quasi-closed diaphragm, which is used to solve the problem of diaphragm breakage in piezoelectric MEMS speakers with non-closed diaphragms, while maintaining a relatively high SPL (about 105 dB in the high-frequency range) and a relatively low amplitude (about 10 μm). Lee et al. [18] used piezoelectric lead lanthanum zirconate titanate (PLZT) ceramics coated with indium tin oxide (ITO) to fabricate a fully transparent transducer with a glass diaphragm, ensuring unobstructed visibility while maintaining the device's functionality. This piezoelectric speaker can deliver excellent sound output, in which the SPL reaches 105 dB at the resonance frequency (5.6 kHz) with an input of only 5 V of peak-to-peak voltage.

At present, there are some typical equations characterizing the acoustic parameters of the microspeakers. Xu et al. [19] studied the elastic diaphragm for pneumatic vibration isolators and derived the close-formed solution for the stiffness of the diaphragm under working conditions using the Mooney-Rivlin model and the theory of elastomers. Lucas et al. [20] investigated the changing rule of inorganic silicon thin films under in-plane and out-of-plane loads and fitted the experimental-simulation data to obtain a linear relationship with F_0 and in-plane loads and a quadratic relationship with F_0 and out-of-plane loads. Kim et al. [21] described the changing rule of rubber and resin diaphragms with respect to changes in elastic modulus and thickness through finite element simulation, formula fitting, and actual measurement. Oh [22] calculated the total quality factor (Q_{ts}) from the electrical

impedance curve of a microspeaker and found that Q_{ts} is only related to and is proportional to F_0 . In addition, the change of frequency response in the vicinity of F_0 is independent of the type and thickness of polymer diaphragms; in fact, it is mainly influenced by F_0 . In another study by this author [23], the influences of material type and thickness of polymer diaphragms on F_0 , FR, and IMP curves were reported. It was found that for all materials investigated in this study, with the increase of diaphragm thickness, the first peak in IMP curves shifts right and the peak value decreases. Oh et al. [24] also reported the influence of diaphragm pattern on its tensile strength and the changing rule of the number of diaphragm patterns and its tensile strength to the F_0 of the microspeakers.

As a typical kind of polymer, rubber has hyperelasticity and can be deformed in a large range without failure. Rubber is a kind of elastomer with a relatively low glass transition temperature (T_g), making it in the high-elastic state at room temperature. Yang et al. [25] and Dong et al. [26] created seals by compounding rubber with fabric, which were used for aircraft cabin door sealing structures. Han et al. [27,28] conducted in-depth studies on vulcanization performance, aging resistance, peeling performance, and other mechanical properties of rubber. Due to the characteristics mentioned above, rubber diaphragms have been gradually applied in microspeakers with large amplitude. Ethyl acrylate rubber (AEM) is a kind of heat- and fluid-resistant elastomer and is suitable for flexible applications in dampers and seals [29]. In terms of the magnitude of elastic modulus in the linear elastic range (E), the values of PEEK [30], TPEE [31], and rubber [32,33] are approximately 1 GPa, 100 MPa, and 10 MPa, respectively. When PEEK and TPEE are used as diaphragm materials, to enhance damping performance, a three-layered laminated composite diaphragm is employed, with an acrylic or silicone adhesive layer in the middle between the outer layers of PEEK/TPEE. Although the E of the adhesive layer is lower than that of PEEK/TPEE, the overall E of the composite diaphragm remains high [34]. The low E and hyperelasticity of rubber materials determine that they have a larger amplitude margin during vibration, thus achieving better sound quality. In contrast, PEEK material has poor elasticity; when large excursions are applied, larger surround width and depth are required to withstand the deformation; hence PEEK material cannot meet the needs for large amplitudes, smaller-sized microspeakers. The advantages of rubber as a material for microspeaker diaphragms mainly include appropriate E and F_0 , excellent damping performance with a high R_{ms} , and at the same time, effectively preventing diaphragm rupture under large excursions, with X_{max} well meeting the existing demands.

At present, existing diaphragm materials generally have a high modulus, poor damping performance, and are prone to rupture under large excursion vibrations, which cannot meet people's demand for speakers with large amplitude and low distortion. In response to this issue, this paper first proposes a high-performance AEM rubber diaphragm based on the third-generation diaphragm materials, using a relatively mature solvent casting and thermoforming method for the vulcanization and molding of diaphragm components, and assembling microspeaker drivers through conventional production lines. The prepared microspeaker drivers have the performance of large amplitude and high damping, which is superior to that of

speakers prepared with traditional PEEK and TPEE diaphragms. Meanwhile, based on the changes in E and thickness of the diaphragm, key parameters K_{ms} and Q_{ms} are calculated to determine the changing rule of F_0 and R_{ms} of the microspeaker with E . This provides a basis for tuning F_0 and TS parameters of the microspeaker through the elastic modulus of the diaphragm material.

2. Experimental

2.1. Materials and manufacturing process

In this study, AEM rubber (Vamac-G) was used as the diaphragm material and was purchased by Du Pont China Holding Co., Ltd. The fillers for AEM rubber were mainly a vulcanizing agent—N,N'-Dicinnamylidene-1,6-hexanediamine supplied by Zhengzhou Acme Chemicals Co., Ltd., talcum powder supplied by Qingdao Lukuang Talcum Powder Co., Ltd., and zinc phosphate supplied by Changzhou Akede New Materials Technology Co., Ltd. The addition ratio of N,N'-Dicinnamylidene-1,6-hexanediamine was 2 phr (phr denotes per hundred rubber). According to the increasing addition ratio of fillers, the samples with a thickness of 90 μm after molding were labeled as AEM-90-1, AEM-90-2, AEM-90-3, AEM-90-4, and AEM-90-5, respectively. Among them, AEM-90-3 was mixed with talcum powder with a filling ratio of 20 phr; the others were mixed with zinc phosphate with filling ratios of 5 phr, 10 phr, 15 phr, and 25 phr, respectively. Based on the filler addition ratio of AEM-90-4, the thickness was adjusted to 80 μm and 100 μm , and the molded samples were labeled as AEM-80-4 and AEM-100-4, respectively.

The diaphragm forming process is divided into two procedures, that is, solvent casting and thermoforming. Firstly, following the commercial molding process, AEM was dissolved, fillers and adhesives were added to the solution and mixed evenly, the coating was formed on the release film after the solvent had been evaporated, and another release film was attached to the coating. After removing one side of the release paper, the rubber film was pre-baked with baking parameters of 150 $^{\circ}\text{C}$ for 3 min. Secondly, the rubber film with the other side of the release paper removed is molded using the thermoforming process [35]. Depending on the specific requirements, different patterned molds were used to transfer the specific pattern shapes onto the rubber film. The thermoforming process parameters are a holding pressure temperature of 190 $^{\circ}\text{C}$, a holding pressure time of 100 s, a heating time of 177 s, and a cooling time of 78 s.

The center parts of the as-prepared diaphragms with steel rings were cut by laser, the dome was attached to the diaphragm by adhesives, and the steel ring was removed. Then, more adhesives were applied on the edges of the diaphragms, the frame and voice coil were fixed, and the diaphragm-voice coil adhesive was also applied. The magnetic circuits, including magnets, top plates, and yokes, were also glued by corresponding adhesives. Finally, the microspeaker drivers were assembled with all components with corresponding adhesives.

The procedural photos and flow charts of the diaphragm forming and the assembling of the microspeakers are demonstrated in **Figure 1**.

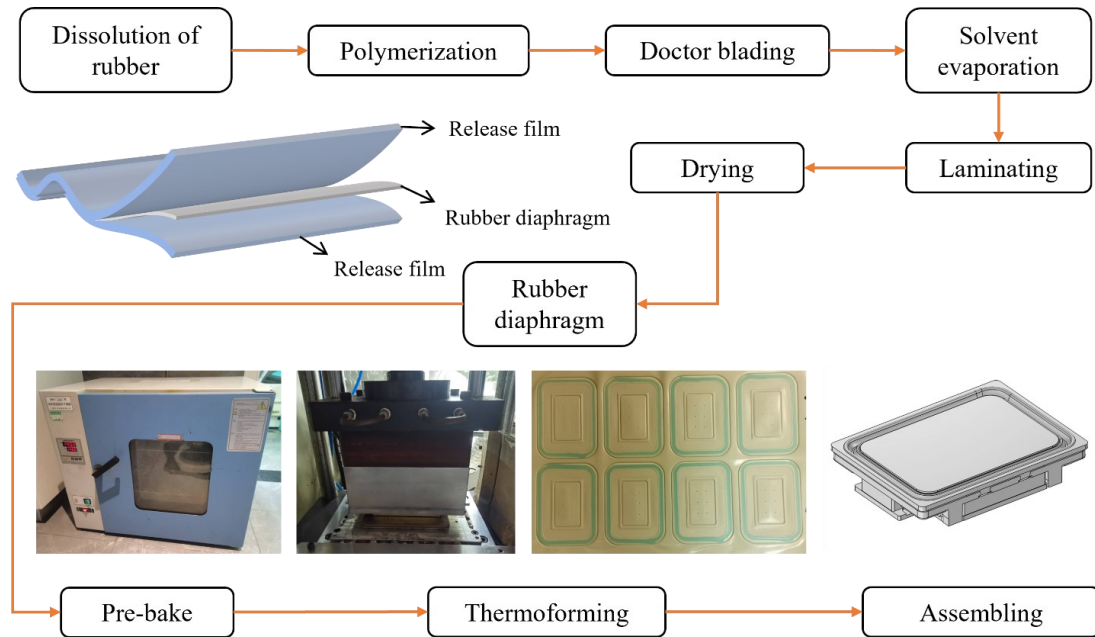


Figure 1. Schematics of diaphragm forming and the assembling of microspeakers.

2.2. Characterization and testing of diaphragms and microspeakers

Through the pre-bake process in Section 2.1, the diaphragm was further formed by the thermoforming process with a flat plate instead of die heads. After the diaphragm was fully cured, it was cut and sampled, and the cut samples were fixed on a universal testing machine for uniaxial tensile testing; Fourier Transformed Infrared Spectroscopy (FTIR) was conducted on the fractured samples to validate the compositions of each sample.

The microspeaker drivers prepared from Section 2.1, except for the diaphragm material, are completely identical in other materials, design, and manufacturing process. Soundcheck test [36], small-signal Klippel test, and large-signal Klippel test were implemented for microspeaker drivers, with four samples made from each composition of diaphragm material. The results obtained were averaged to characterize the amplitude and damping performance of the microspeakers.

3. Results and discussions

3.1. FTIR of diaphragm materials

AEM is an ethylene copolymer with an acrylic acid content of 8% to 40%, which is obtained by polymerizing ethylene and methyl acrylate using oxygen or peroxide as an initiator under high pressure and heat, with the structural formula shown in **Figure 2** [37,38]. The infrared spectra of the diaphragm samples are shown in **Figure 3**.

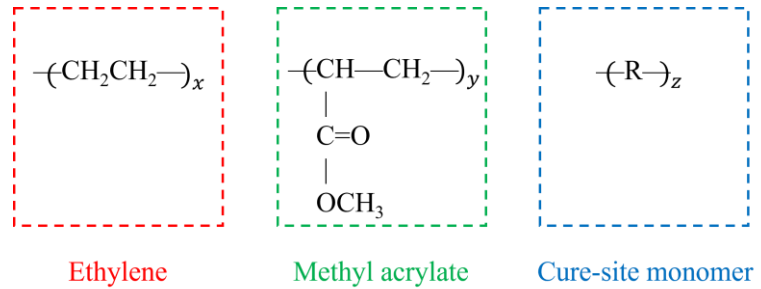


Figure 2. Typical molecular structures of AEM.

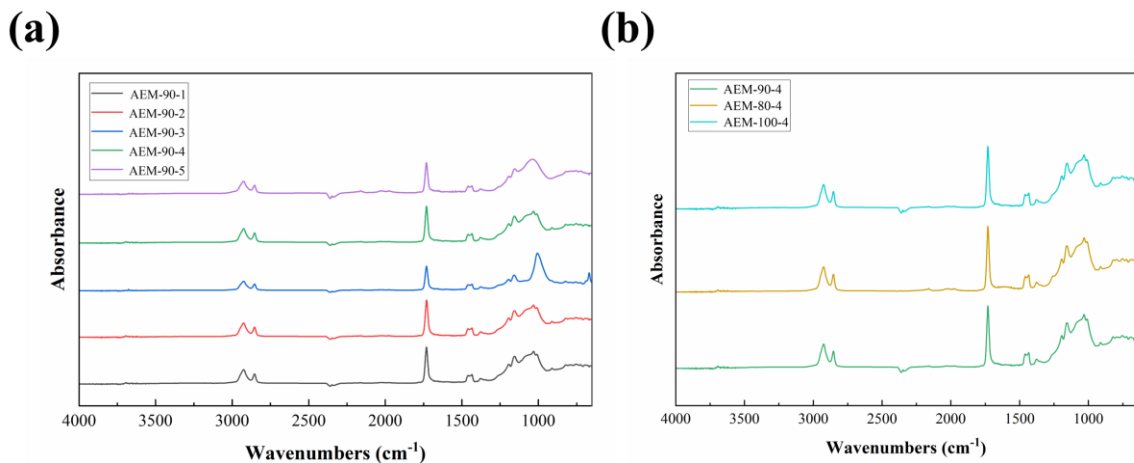


Figure 3. FTIR spectra of (a) samples with thicknesses of 90 μm ; (b) samples with different thicknesses.

From the results of **Figure 3a**, the spectra of AEM-90-1 to AEM-90-5 show the main absorption peaks in the functional group region (4000 cm^{-1} to 1300 cm^{-1}) at the same positions, indicating that their main compositions are the same; the band positions, shapes, and intensities in the fingerprint region (1300 cm^{-1} to 600 cm^{-1}) are slightly different, indicating that there are minor differences in the specific formulations of each.

Specifically, the wavenumbers at 2925 cm^{-1} and 2854 cm^{-1} correspond to the symmetric and asymmetric stretching vibration absorption peaks of $-\text{CH}_2-$, which are associated with aliphatic hydrocarbons; the wavenumber at 1727 cm^{-1} corresponds to the stretching vibration absorption peak of $\text{C}=\text{O}$, which is associated with aliphatic carboxylic acids; the wavenumber at 1432 cm^{-1} corresponds to the stretching vibration absorption peak of $\text{C}-\text{H}_3$, and the wavenumber at 1155 cm^{-1} corresponds to the stretching vibration absorption peak of $-\text{O}-\text{CH}_3$ [39]. The above results indicate that the characteristic peaks of AEM rubber are very obvious in all AEM-90-1 to AEM-90-5 samples, and their main compositions are AEM rubber.

The spectra of AEM-90-1, AEM-90-2, AEM-90-4, and AEM-90-5 exhibit antisymmetric stretching vibration absorption peaks for $-\text{PO}_4-$ in the wavenumber range of 1100 cm^{-1} to 1050 cm^{-1} , with slightly different intensities of the absorption peaks for each sample, indicating that the powder materials are inorganic phosphates [40,41], but the amounts added are different. The spectrum of AEM-90-3 shows an antisymmetric stretching vibration absorption peak for $\text{Si}-\text{O}$ in the wavenumber range of 1100 cm^{-1} to 1000 cm^{-1} , indicating that the powder material is silicate [42,43].

From the results of **Figure 3b**, the spectra of the three samples are essentially consistent in the functional group region, indicating that there are no significant differences in their material formulations, and the main composition is AEM. In the fingerprint region, all three samples have an antisymmetric stretching vibration absorption peak for $\text{—PO}_4\text{—}$ at the wavenumber range of 1100 cm^{-1} to 1050 cm^{-1} , indicating the addition of inorganic phosphates to AEM.

3.2. Mechanical behavior of diaphragms

As described in Section 2.2, in accordance with the standards ISO 527-1:2019 and ISO 527-3:2018, the fully cured diaphragm samples were cut into a size of $20\text{ mm} \times 100\text{ mm}$. The cut samples were fixed onto a universal testing machine with an initial gauge length of 50 mm . The testing machine was started, and a uniaxial tensile test at a speed of 200 mm/min was performed until the sample fractured. The displacement and load were recorded, and the E of the samples was calculated through the testing machine by Equation (1).

$$E = \frac{\sigma_{0.25} - \sigma_{0.05}}{0.0025 - 0.0005} = 500(\sigma_{0.25} - \sigma_{0.05}) \quad (1)$$

where $\sigma_{0.25}$ and $\sigma_{0.05}$ denote the nominal stress of the samples when the nominal strain is 0.25% and 0.05% , respectively. The E , elongation at break ($EAB\%$) and tensile strength (TS) were obtained and illustrated in **Figure 4**.

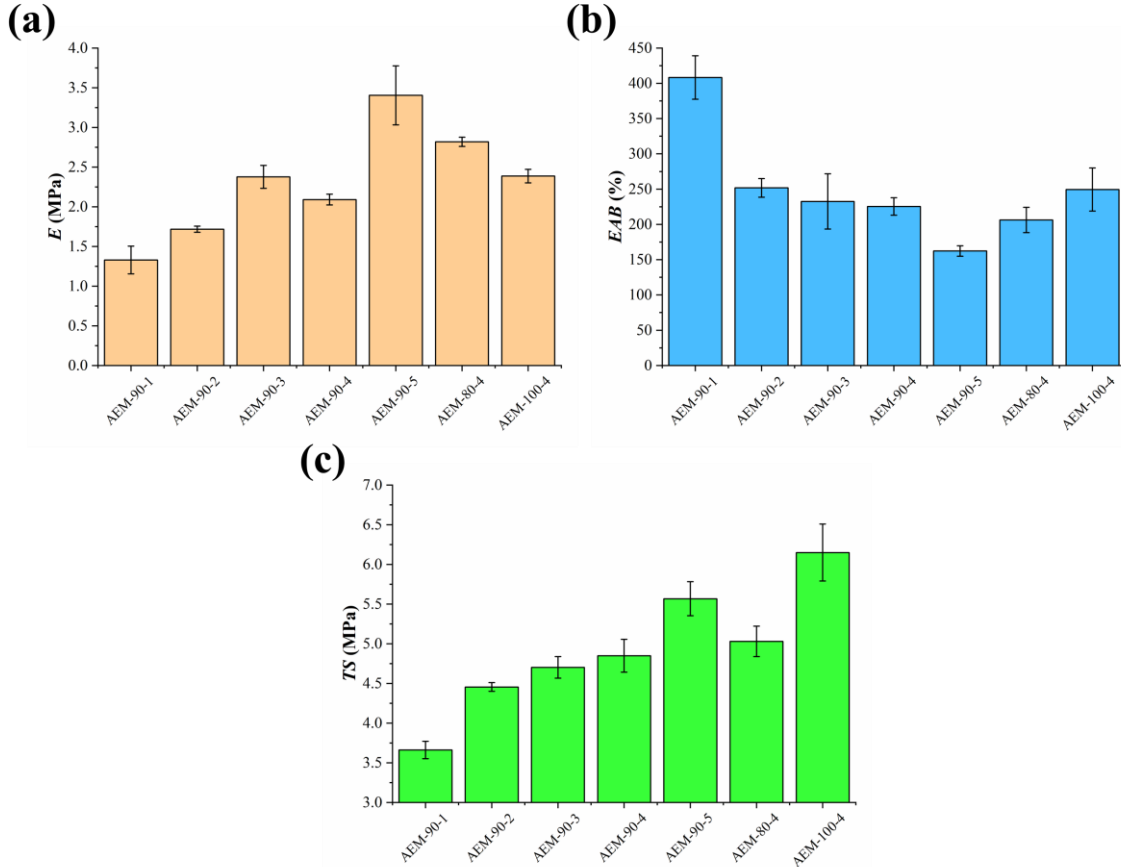


Figure 4. Bar charts of all samples: (a) E ; (b) $EAB\%$; (c) TS .

From the results of **Figure 4a**, AEM-90-1 has the lowest E , while AEM-90-5 has the highest E , corresponding to the powder loading in the formulation from the lowest to the highest; the difference between AEM-90-3 and AEM-90-4 may be due to the different types of powders used. From AEM-80-4, AEM-100-4 to AEM-90-4, the E decreases in sequence. From the results of **Figure 4b**, AEM-90-5 has the lowest $EAB\%$, and from AEM-90-5, AEM-80-4 to AEM-100-4, the $EAB\%$ increases in sequence. From the results of **Figure 4c**, AEM-90-1 has the lowest TS , while AEM-90-5 has the highest TS , with AEM-80-4 slightly lower than AEM-90-4 and AEM-100-4 slightly higher than AEM-90-4. Based on the above analysis, from AEM-90-1 to AEM-90-5, the different loadings and types of powders lead to an increase in E and TS and a decrease in $EAB\%$, which is in line with the material regulation rules. At the same time, as similar compositions, AEM-80-4 and AEM-100-4 have slightly higher E and TS compared to AEM-90-4, with $EAB\%$ remaining almost the same.

The mechanical properties discussed above influence the sound quality and low-frequency performances of the microspeakers made by the rubber diaphragm samples. Firstly, in terms of E , AEM-90-5 with the highest E helps to reduce separated vibrations and makes sound signals more precisely recovered, which will be validated in the following sections. Although an extremely high E will impair the maximum excursion, compared to other polymer-based diaphragms, the E of AEM-90-5 is sufficiently low. Secondly, in terms of $EAB\%$, AEM-90-5 with the lowest $EAB\%$ could keep intact in high-amplitude vibrations, proving that all the other samples have enough stability of the sound quality. Finally, in terms of TS , since AEM-90-1 with the lowest TS is not prone to failure under large signals, and the low-frequency performances are fair, all the other samples have enough reliability and stability in the low-frequency range.

3.3. Soundcheck results of microspeaker drivers

To evaluate the acoustic performance of the speakers, a 10 cm baffle was used to conduct Soundcheck tests on the microspeaker samples. Through the Soundcheck tests, FR curves, IMP curves, and THD curves [44,45] were obtained; F_0 could also be further derived from the IMP curve.

3.3.1. FR

The FR data could be obtained directly by the Soundcheck system and software; see **Figure 5** for FR curves of all samples.

The FR curve is a plot of SPL (also known as sensitivity) in terms of frequency. The commonly used values FR500 and FR2000 refer to the SPL at frequencies of 500 Hz and 2000 Hz, respectively, with the unit dB. From **Figure 5a**, it can be seen that in the low-frequency range ($F < 1000$ Hz), the SPL of all samples is essentially the same, and the curves are relatively smooth; in the mid-frequency range ($1000 \text{ Hz} < F < 10,000$ Hz), the SPL of the samples is around 95 dB; in the high-frequency range ($F > 10,000$ Hz), differences begin to occur in SPL, among which AEM-90-5 has the least fluctuation and higher sensitivity in the second resonance region, indicating that a higher powder loading is beneficial to the improvement of the FR performance of the diaphragm material. From **Figure 5b**, it can be seen that in the low-frequency range, AEM-100-4 has the highest SPL, while AEM-80-4 has the

lowest SPL; in the high-frequency range, the second resonance region of AEM-100-4 is not significant, and the SPL even exceeds that of the low-frequency range. Referring to **Figure 4**, since the E of AEM-80-4 is higher than that of AEM-100-4, high-frequency vibrations are inhibited, resulting in a smoother FR curve and a lower SPL. Furthermore, since the $EAB\%$ and TS of AEM-100-4 are higher than those of AEM-80-4, AEM-100-4 could withstand higher input voltage and result in a higher SPL at a high-frequency range, especially at 19,000 Hz.

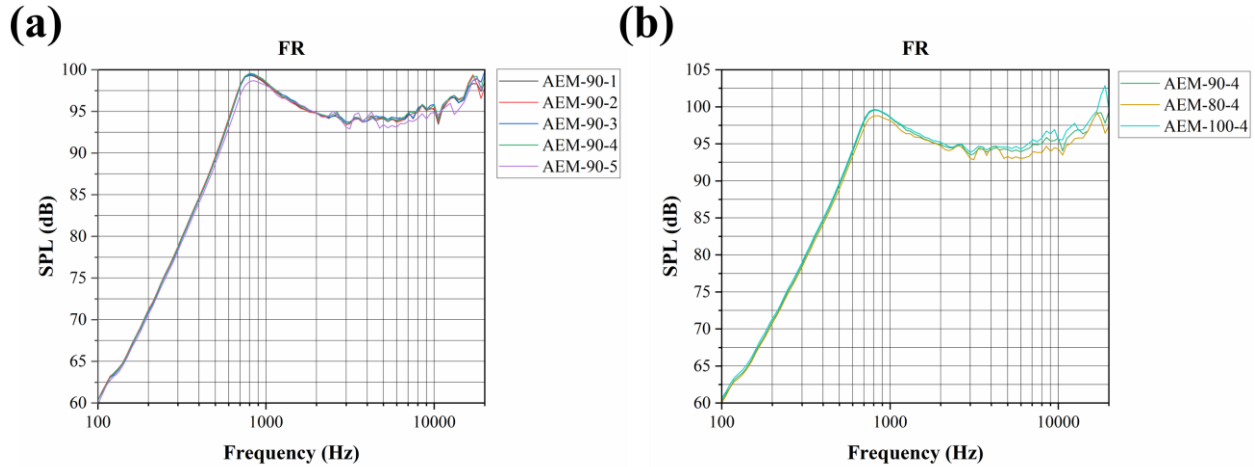


Figure 5. FR curves of (a) samples with thicknesses of 90 μm ; (b) samples with different thicknesses.

Compared to other polymer-based diaphragms, the rubber diaphragms fabricated in this study exhibit excellent FR performances. The SPL of the polyester and polystyrene diaphragm-based dynamic loudspeaker [46] can reach 88 dB at the resonance zone and 92 dB at the second plateau. The SPL of a polyimide diaphragm-based flexible planar loudspeaker [47] can reach 70 dB at a low-frequency range. The SPL of the polyethylene naphthalene (PEN) and polyethylene terephthalate (PET) diaphragm-based electrostatic speaker with a thickness of 25 μm [48] can reach 40 dB and 50 dB, respectively. The SPL of dielectric silicone rubber film-based electroactive polymer loudspeakers [49] can reach 80 dB.

3.3.2. IMP

The IMP curves of all samples could also be obtained by Soundcheck, as shown in **Figure 6**. Also, the F_0 of each sample is obtained from the corresponding IMP curve, as shown in **Figure 7**. The IMP curve describes the relationship between electrical impedance and frequency. The most frequently used value is IMP2000, which corresponds to electrical impedance at 2000 Hz. F_0 is the frequency corresponding to the first maximum value of electrical impedance, which could be directly obtained by the software and has a relationship with TS parameters (see Equation (2), where K_{ms} and M_{ms} are the mechanical stiffness of the driver suspension and the imported mechanical mass of the driver diaphragm assembly, respectively). F_0 is independent of impedance value and is only related to the position where the first maximum value appears on the IMP curve. The F_0 of drivers without back chambers is relatively low (400–600 Hz); the F_0 of drivers with back chambers is usually more than 700 Hz.

$$F_0 = \frac{1}{2\pi} \sqrt{\frac{K_{ms}}{M_{ms}}} \quad (2)$$

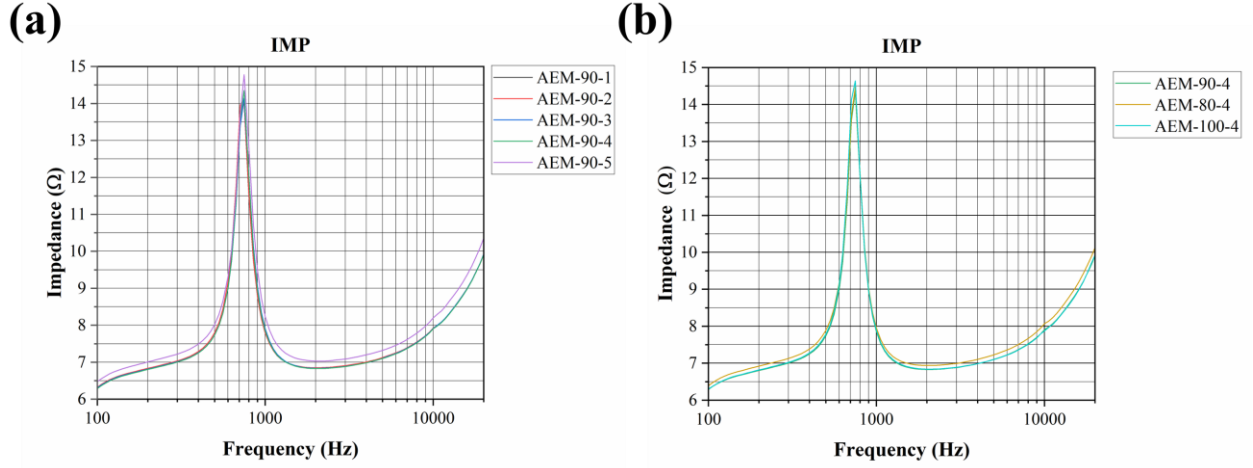


Figure 6. IMP curves of (a) samples with thicknesses of 90 μm ; (b) samples with different thicknesses.

Through the IMP curves in **Figure 6a**, we can observe that from AEM-90-1 to AEM-90-5, the position of the first maximum value of the curve shifts towards the positive direction of the horizontal axis, corresponding to an increase in F_0 ; at the same time, the first maximum value (electrical impedance) gradually increases. This indicates that as the powder loading in AEM rubber increases, both F_0 and the impedance value are increasing. From **Figure 6b**, it can be seen that AEM-80-4 has the highest maximum electrical impedance.

From **Figure 7**, it can be seen that AEM-90-5 has the highest F_0 . Although lowering the F_0 helps to improve low-frequency performance, if it is too low, the reliability margin of the microspeaker will decrease. This is due to the fact that for low-frequency vibrations, large excursions could result in the increase of stress and strain of the diaphragm and the suspension; meanwhile, the nonlinear distortions and more complex structures also lead to the reduction of the reliability margins. According to the application requirements, the F_0 meets the specifications. Based on information from mature microspeaker products on the market, this parameter value is within the normal range, on the lower side, indicating that the speaker has excellent low-frequency performance. By comparing **Figure 7** with **Figure 4a**, it can be observed that the changing rule of the F_0 for each sample is very close to that of the E , except that AEM-90-4 has a lower E than AEM-90-3 and AEM-80-4, while the F_0 is higher than that of AEM-90-3 and AEM-80-4. The potential reason for AEM-90-3 having a higher E than AEM-90-4, while having a lower F_0 , is the difference in the types of powder used.

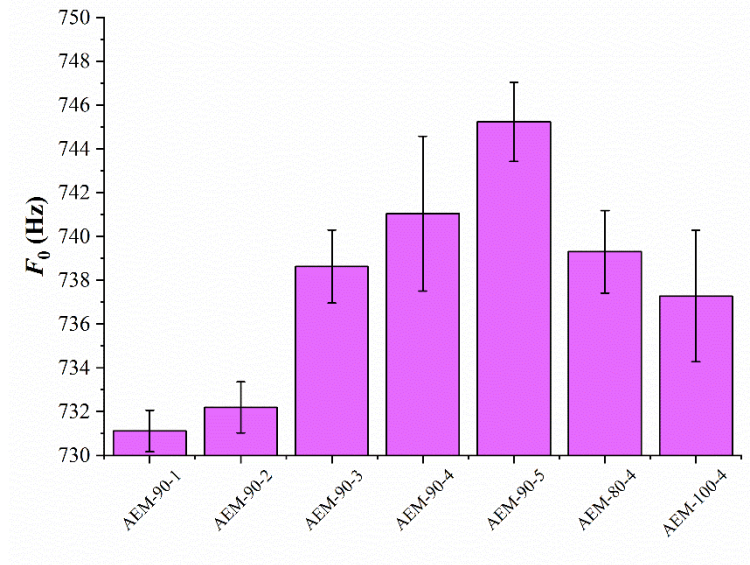


Figure 7. F_0 of all samples.

3.3.3. THD

The THD curves of all samples could also be obtained by Soundcheck, as shown in Figure 8. When the input signal is sinusoidal, the nonlinearity of the ratio of the harmonic signal to the total signal in the output signal is characterized by harmonic distortion; the harmonic distortion referred to as THD% is expressed as the ratio of the effective value of the signal distortion components to the effective value of the total output signal. The typical value of the THD curve is THD₂₆₅, which refers to THD% at 265 Hz. THD%, or THD, THD_R, is calculated as [50–52] Equation (3).

$$\text{THD}\% = \frac{\sqrt{H_2^2 + H_3^2 + \dots + H_N^2}}{\sqrt{H_1^2 + H_2^2 + H_3^2 + \dots + H_N^2}} \times 100\% \quad (3)$$

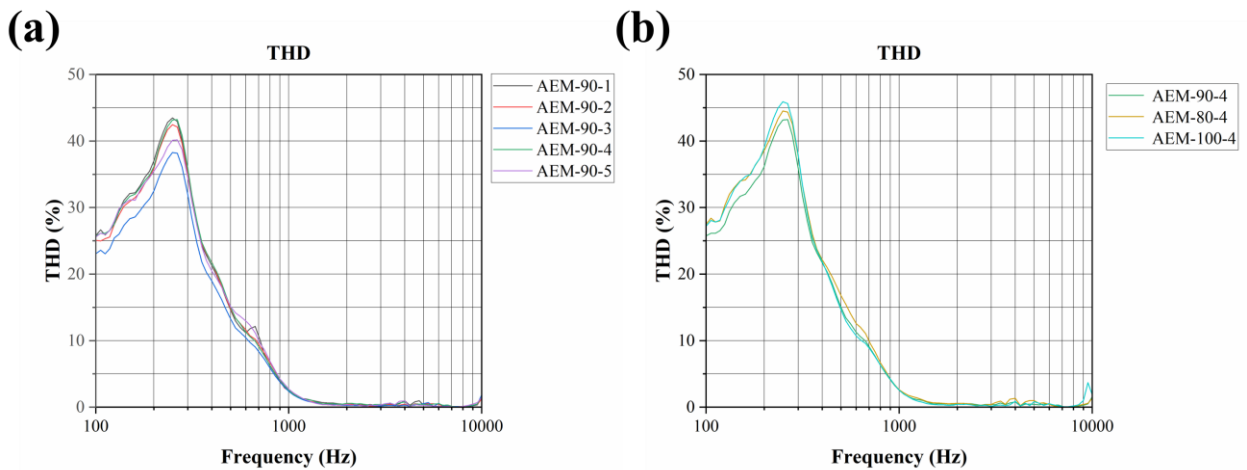


Figure 8. THD curves of (a) samples with thicknesses of 90 μm; (b) samples with different thicknesses.

From Figure 8a, it can be observed that in the THD curves of AEM-90-3 and AEM-90-5, the first maximum value does not exceed 40%, while the THD% of the other samples exceeds 40% to varying degrees. The THD% of AEM-90-3 and AEM-

90-5 is less than 10% at F_0 , while others exceed 10%. From **Figure 8b**, it can be seen that the THD% of AEM-90-4, AEM-80-4, and AEM-100-4 all exceed 40%, and correspondingly, the THD% of all samples exceed 10% at F_0 . From the THD% data of the samples, it is indicated that AEM-90-3 and AEM-90-5 have the best anti-distortion performance. It can be concluded that a high loading of inorganic phosphates and a medium content of inorganic silicates contribute to the improvement of the anti-distortion performance of microspeakers.

In the FR, IMP, and THD curves of the above samples, there are several representative values: FR500, FR2000, IMP2000, and THD265. The comparison of these values for each sample is made simultaneously, and the results are presented in **Table 1**.

Table 1. Acoustic parameters of all samples.

Samples	F_0 (Hz)	FR500 (dB)	FR2000 (dB)	THD265 (%)	IMP2000 (Ω)
AEM-90-1	731.12	89.54	94.73	42.25	6.86
AEM-90-2	732.20	89.55	94.81	42.27	6.84
AEM-90-3	738.63	89.34	94.91	39.11	6.84
AEM-90-4	741.04	89.35	94.83	42.73	6.83
AEM-90-5	745.23	88.75	94.77	39.82	7.04
AEM-80-4	739.31	88.91	94.77	43.77	6.95
AEM-100-4	737.28	89.60	95.26	43.55	6.85

From **Table 1**, it can be seen that microspeakers made by AEM-90-1 and AEM-90-2 have higher FR500, while AEM-90-3 and AEM-90-4 have higher FR2000, and AEM-90-5 has lower FR500 and higher FR2000, indicating that AEM-90-5 has a larger change in SPL from low-frequency to mid-frequency. Combined with the results of **Figure 5a**, the SPL changes from mid-frequency to high-frequency are smaller, and the overall fluctuations are minimal. In terms of THD265, AEM-90-3 and AEM-90-5 have the best anti-distortion performance; considering the IMP2000 values, AEM-90-5 has the highest electrical impedance. It can be concluded that reasonably increasing the powder loading helps to improve the impedance and anti-distortion performance of microspeakers; among the samples studied in this paper, AEM-90-5 has the best comprehensive performance. In addition, it can be observed that the microspeaker made by AEM-100-4 has higher FR500 and FR2000, while AEM-90-4 has lower THD265 and IMP2000. This indicates that increasing the diaphragm thickness helps to enhance the sensitivity of microspeakers.

3.4. Klippel results of microspeaker drivers

To evaluate the nonlinear behavior of the microspeakers and the vibration characteristics of the diaphragm, the microspeaker products are further tested by the Klippel R&D System, which is usually classified into a small signal test and a large signal test.

3.4.1. Small-signal TS parameters

Small signal Klippel test is mainly used to evaluate microspeaker performances in the linear range. The TS parameters could be obtained by the input of small signals

where the vibration of the diaphragm is approaching ideally linear vibration. Using the laser measurement method, the microspeaker drivers were fixed to specific fixtures, and the Klippel R&D system was activated. The sample's excursion and vibration velocity are obtained through laser sensor scanning, and the TS parameters of the sample are ultimately calculated.

Small signal TS parameters consist of electrical parameters (subscript “es”), mechanical parameters (subscript “ms”), and acoustic parameters (subscript “as”). Through the Klippel R&D System, the TS parameters were directly obtained, as listed in **Table 2**.

Table 2. Main small-signal TS parameters of all samples.

Samples	f_s (Hz)	R_{ms} (kg/s)	C_{ms} (mm/N)
AEM-90-1	775.90	0.098	0.421
AEM-90-2	771.58	0.097	0.421
AEM-90-3	787.18	0.103	0.415
AEM-90-4	779.63	0.112	0.410
AEM-90-5	830.37	0.134	0.357
AEM-80-4	777.58	0.100	0.412
AEM-100-4	793.45	0.102	0.403

where f_s is the resonance frequency of the speaker driver in free space, which is generally slightly higher than the F_0 measured without the back chamber. C_{ms} is the mechanical compliance of the driver suspension. R_{ms} is the mechanical resistance of total driver losses, which is mainly determined by the diameter of the orifice. The material of the diaphragm and some auxiliary adhesives can also influence R_{ms} . We have

$$R_{ms} = \frac{1}{Q_{ms}} \sqrt{M_{ms} K_{ms}} \quad (4)$$

where Q_{ms} is the mechanical Q-factor of the driver in free air, M_{ms} is the imported mechanical mass of the driver diaphragm assembly, and K_{ms} is the mechanical stiffness of the driver suspension.

From the results in **Table 2**, it can be seen that the f_s of all samples is higher than F_0 ; AEM-90-5 has the highest R_{ms} among all samples, while C_{ms} is the lowest. Relating this to the mechanical properties of AEM-90-5, it can be inferred that the higher E and lower C_{ms} of the diaphragm contribute to the higher F_0 and R_{ms} of the microspeaker.

R_{ms} is an important indicator of the damping performance of the diaphragm material. Increasing R_{ms} can effectively reduce THD% and improve the sound quality of microspeakers. A comparison of E , F_0 , and R_{ms} for each sample is presented in **Table 3**.

From **Table 3**, it can be observed that when the thickness is the same, increasing the powder loading in the rubber diaphragm gradually increases its E , and both F_0 and R_{ms} of the microspeakers show a gradual increase. Among them, AEM-90-4 shows a decrease in E and an increase in F_0 and R_{ms} compared to AEM-90-3, which is related

to the different types of powder used. In addition, it can be seen that from AEM-80-4 to AEM-90-4, E decreases significantly, F_0 slightly increases, and R_{ms} increases considerably. From AEM-80-4 to AEM-100-4, E decreases significantly, but the decrease in F_0 and R_{ms} is not apparent. According to Equation (2), F_0 is directly proportional to the square root of M_{ms} and K_{ms} ; when the thickness of the rubber diaphragm increases while keeping the density constant, M_{ms} increases, and thus F_0 increases. As the E of the rubber membrane increases, K_{ms} increases, and thus F_0 increases. According to Equation (4), R_{ms} is directly proportional to the square root of M_{ms} and K_{ms} , and is inversely proportional to Q_{ms} . For AEM-90-1, AEM-90-2, AEM-90-4, and AEM-90-5, the thickness of the rubber diaphragm remains unchanged, but the density increases, so E increases, and thus R_{ms} increases; from AEM-90-4 to AEM-80-4, the thickness of the rubber diaphragm decreases, E increases, F_0 decreases, and R_{ms} decreases, indicating that the thickness has a more significant effect on R_{ms} than E ; from AEM-90-4 to AEM-100-4, the thickness of the rubber diaphragm increases, E increases, F_0 decreases, and R_{ms} decreases, indicating that a decrease in density has a more significant effect on R_{ms} than E . Based on the above discussions, the following changing rules can be derived: (1) When the thickness is kept constant, as the powder loading increases, the density increases, and both F_0 and R_{ms} increase with the increase of E ; (2) When the thickness changes, M_{ms} , the combination of thickness and density, has a more significant impact on F_0 and R_{ms} than E .

Table 3. Acoustic parameters of all sample corresponding to E .

Samples	E (MPa)	F_0 (Hz)	R_{ms} (kg/s)
AEM-90-1	1.55	731.12	0.098
AEM-90-2	1.72	732.20	0.097
AEM-90-3	2.38	738.63	0.103
AEM-90-4	2.09	741.04	0.112
AEM-90-5	3.40	745.23	0.134
AEM-80-4	2.82	739.31	0.100
AEM-100-4	2.39	737.28	0.102

3.4.2. Large-signal parameters

The large signal Klippel test is mainly used to evaluate microspeaker performances in the nonlinear range. To be more specific, the vibration of the diaphragm is nonlinear, harmonic distortion and compression occur with the input of a high-voltage signal, and the amplitude parameters could be obtained.

The large-signal parameters obtained from the Klippel test are mainly designated as excursions, and the maximum excursion of the voice coil through all frequency ranges is called X_{max} , or amplitude. X_{max} is also defined as the maximum excursion of the voice coil when THD% = 10%. Due to the limited data, only excursion curves of samples AEM-90-1, AEM-90-2, AEM-90-3, AEM-90-4, and AEM-90-5 are shown; see **Figure 9**.

As shown in **Figure 9**, the upper excursion of AEM-90-2 can reach 0.7 mm; in terms of excursion symmetry, the behavior of AEM-90-3 and AEM-90-5 is better.

Therefore, the X_{\max} and symmetry of AEM-90-5 are the best in all samples listed in **Figure 9**. Moreover, compared to other speaker products in the market mentioned above, the X_{\max} of AEM-90-5 of approximately 0.58 mm is superior to that of TPEE-based microspeakers.

Combining the excursion data mentioned before, an Ashby plot is created for the relationship between the X_{\max} of speakers made with different diaphragm materials and the E of the diaphragm, as shown in **Figure 10**.

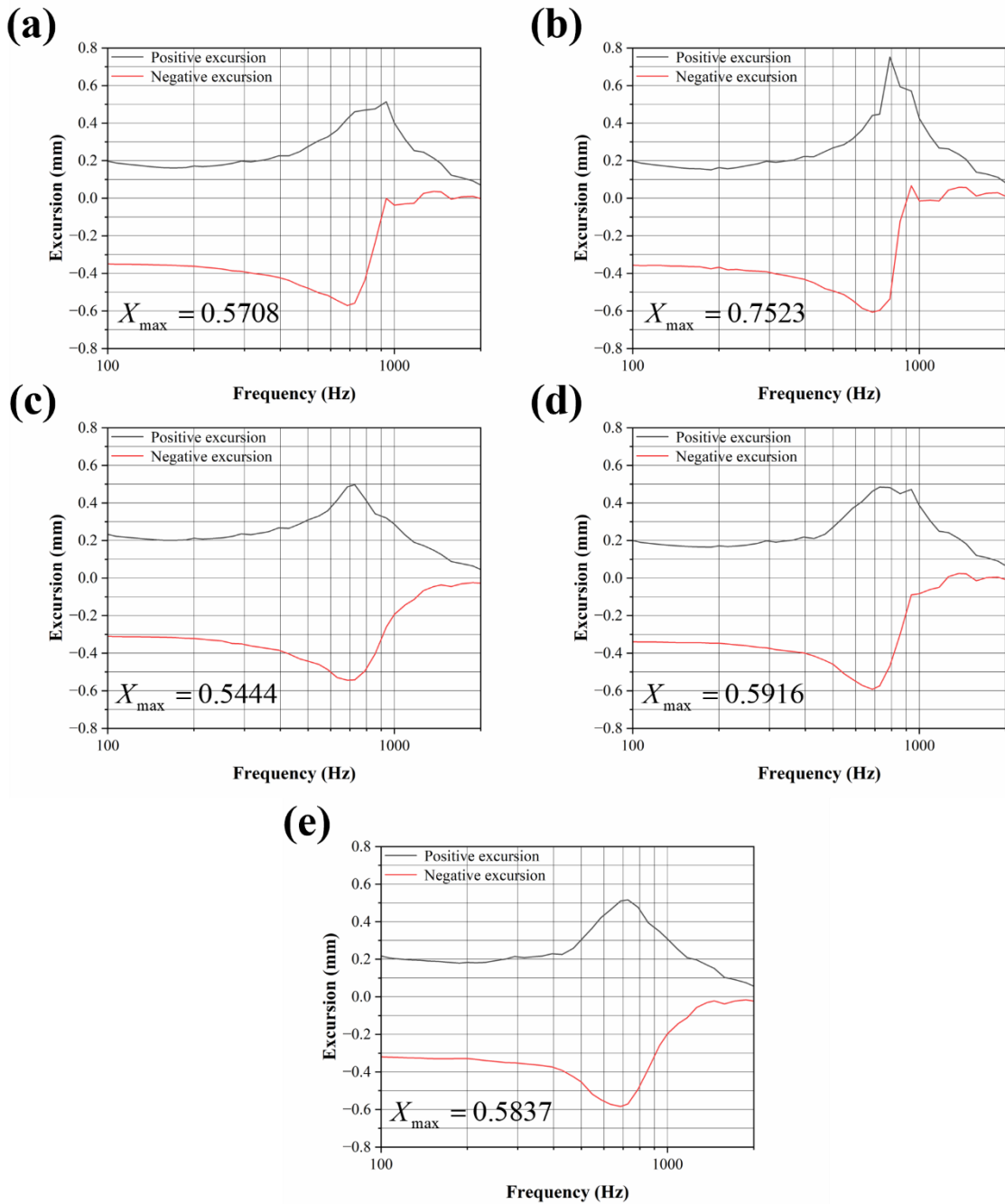


Figure 9. Excursion curves of (a) AEM-90-1; (b) AEM-90-2; (c) AEM-90-3; (d) AEM-90-4; (e) AEM-90-5.

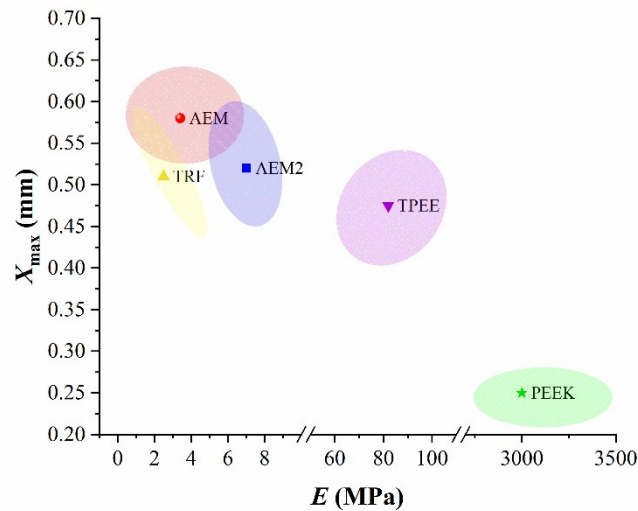


Figure 10. Ashby plot of E and X_{max} of common diaphragm materials.

From **Figure 10**, it can be discovered that the traditional diaphragm material PEEK is located in the lower right corner of the Ashby plot, with the highest E , while the corresponding speaker X_{max} is the lowest; TPEE is located in the middle of the Ashby plot, with a moderate E , and the corresponding speaker X_{max} is improved; TRF is a modified TPEE material made by mixing epoxy resin (hard segment) and rubber (soft segment) in a certain ratio, and compared with TPEE, TRF has a lower E and a slightly higher X_{max} ; AEM is the rubber system studied in this paper, and it has the largest X_{max} and the smallest E . AEM2 is another AEM rubber system, with an X_{max} close to TRF and a slightly higher E . Observing from all the diaphragm materials in **Figure 10**, based on the current and future needs of microspeakers, AEM is the best in terms of comprehensive performance among all the aforementioned materials.

From Soundcheck and Klippel results of microspeakers based on AEM rubber diaphragm samples, we can find that although the acoustic performances of different samples are distinct, some curves may overlap and fluctuate, and some values have significant error bars. The potential sources of experimental error accounting for the above discussions are actually complicated. Firstly, the vulcanization state of the rubber diaphragm influences E and F_0 ; it is likely that a fully vulcanized diaphragm with a higher E exhibits a lower F_0 compared to a partially vulcanized diaphragm with a lower E . Secondly, the testing condition (i.e., the temperature, the humidity, and the placing durations of the diaphragm after vulcanization) could also influence the F_0 and R_{ms} tested. Finally, for each microspeaker fabricated with the same diaphragm, the bonding state and the amount of the adhesives of the whole structure may vary from product to product. Therefore, all the experimental results discussed above have been reasonably selected and averaged, based on a strict control of variables.

3.5. The relationship between the mechanical properties of diaphragms and the acoustic properties of the microspeaker driver

According to the results and discussions in Sections 3.3 and 3.4, the acoustic properties of microspeakers are mainly tested by Soundcheck and Klippel R&D

System. The principal parameters include F_0 , R_{ms} , and THD%, in which F_0 and R_{ms} are core parameters concerning the diaphragm materials, and R_{ms} directly influences THD%. In order to relate F_0 and R_{ms} to characteristic parameters of diaphragm materials, in this section, two significant acoustic parameters, K_{ms} and Q_{ms} , will be calculated through two different methods.

3.5.1. The calculations of K_{ms}

By changing the diaphragm compositions and thicknesses, it is possible to reasonably tune the F_0 and R_{ms} . According to Equation (2), F_0 is inversely proportional to the square root of the M_{ms} and directly proportional to the square root of the K_{ms} . Although the C_{ms} can be directly obtained from the Klippel R&D system, and the values of K_{ms} and C_{ms} are reciprocal to each other, actually, the value of K_{ms} varies at every position along the direction of diaphragm vibration; the value at the equilibrium position is often taken. Based on the definition of K_{ms} , we have

$$K_{ms} = \frac{F}{X} \quad (5)$$

where F and X are load and displacement along the x -axis (perpendicular to the dome), respectively.

The microspeaker described in this paper (**Figure 11a**) is modeled, considering only the vibration system (voice coil, diaphragm, dome and suspension), and excluding other components. The model is exported using Pro/E and then imported into ABAQUS/CAE (**Figure 11b** is the view observed from the positive direction of the x -axis, and **Figure 11c** is the view observed from the negative direction of the x -axis). The material property of the diaphragm is set as the first-order Ogden hyperelastic model (see Equation (6), where S is nominal stress, λ is principal stretch, and μ_1 and α_1 are constitutive parameters).

$$S = \frac{2\mu_1}{\alpha_1^2} (\alpha_1 \lambda^{\alpha_1 - 1} - \alpha_1 \lambda^{-\alpha_1/2 - 1}) \quad (6)$$

The element types of the voice coil, the dome, and the diaphragm (suspension) are C3D10 with 21,549 nodes and 12,294 elements, C3D10 with 39,084 nodes and 19,555 elements, and S4R with 4,896 nodes and 4,717 elements, respectively.

A quasi-static displacement load perpendicular to the diaphragm-dome plane is applied to the voice coil, with a displacement of 0.5 mm ($X = -0.5 \sim 0.5$). Through calculation, the data for $F - X$ is obtained. Then, using Equation (5), the corresponding K_{ms} for each increment step is calculated, and $K_{ms} - X$ is plotted to obtain the K_{ms} curve for all samples, as shown in **Figure 12**. The K_{ms} of all samples at the equilibrium position ($X = 0$) is presented in **Table 4**.

From **Figure 12a**, it can be observed that AEM-90-5 has a larger K_{ms} , while the other four samples have a smaller K_{ms} , which is closely related to the highest powder loading in AEM-90-5. From **Figure 11b**, it can be seen that from AEM-80-4, AEM-90-4, to AEM-100-4, K_{ms} increases in sequence.

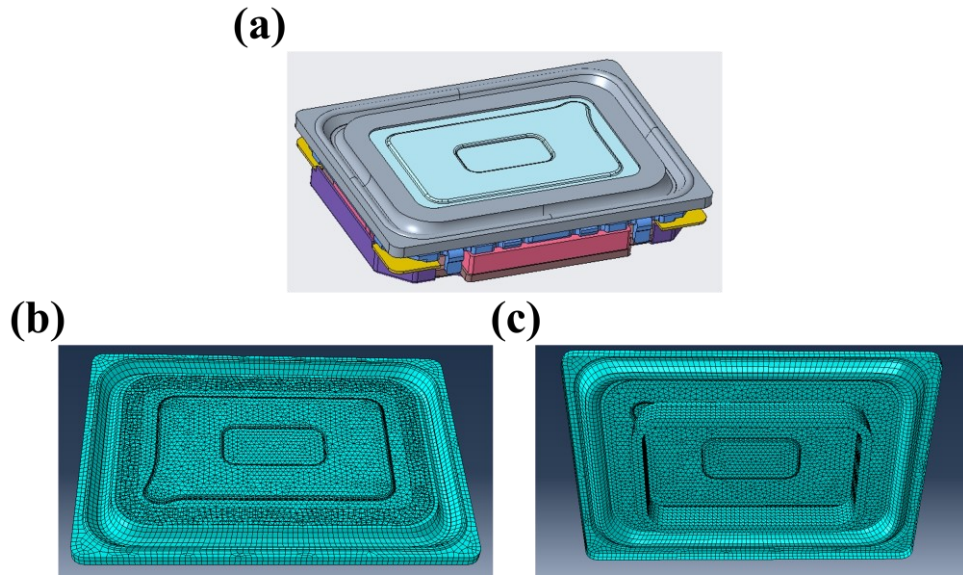


Figure 11. (a) Schematic of the microspeaker described in this study; (b) finite element model of meshed simplified microspeaker (top view); (c) bottom view of (b).

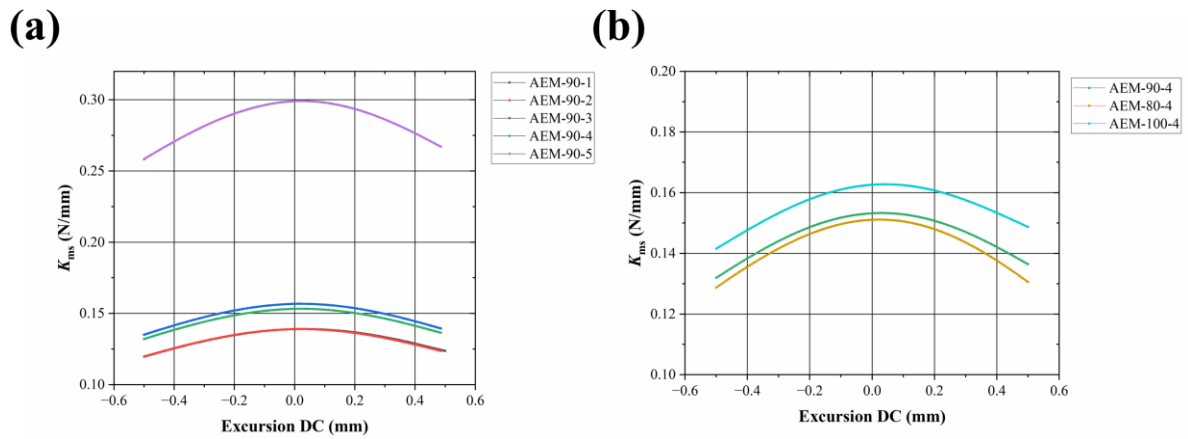


Figure 12. K_{ms} curves of (a) samples with thicknesses of 90 μm ; (b) samples with different thicknesses.

Table 4. Comparison of K_{ms} to E of all samples.

Samples	E (MPa)	K_{ms} (N/mm)	K_{ms}/E (mm)
AEM-90-1	1.55	0.139	0.090
AEM-90-2	1.72	0.139	0.081
AEM-90-3	2.38	0.157	0.066
AEM-90-4	2.09	0.153	0.073
AEM-90-5	3.40	0.299	0.088
AEM-80-4	2.82	0.151	0.054
AEM-100-4	2.39	0.163	0.068

From **Table 4**, it can be seen that for samples with a thickness of 90 μm , although there is a significant difference in E (from 1.55 MPa to 3.4 MPa), the K_{ms} (from 0.139 N/mm to 0.299 N/mm) also increases, and the ratio of the two (K_{ms}/E) only fluctuates between 0.7 and 0.9 mm. Based on Equation (2), Equation (4), and the fact that the

dimensions of K_{ms} and E only differ by a factor of L (length), it can be inferred that when the diaphragm material formulation and thickness are determined, as the E of the diaphragm increases, both F_0 and R_{ms} of the microspeaker will also increase accordingly.

When the thickness of the diaphragm changes (for example, from AEM-90-4 to AEM-80-4 or from AEM-90-4 to AEM-100-4), the ratio of K_{ms}/E also fluctuates between 0.5–0.7mm. Similarly, as the E of the diaphragm increases, both F_0 and R_{ms} of the microspeaker will increase accordingly, but due to the increase in diaphragm thickness, M_{ms} also increases. From AEM-90-4 to AEM-100-4, even though the K_{ms} increased from 0.153 N/mm to 0.163 N/mm, the F_0 actually decreased from 741.04 Hz to 737.28 Hz (Table 3).

3.5.2. The calculations of Q_{ms}

From Equations (2) and (4), it is known that both F_0 and R_{ms} are closely related to the value of K_{ms} . And if we divide R_{ms} by F_0 , we will have

$$\frac{R_{ms}}{F_0} = \frac{\frac{1}{Q_{ms}} \sqrt{M_{ms} K_{ms}}}{\frac{1}{2\pi} \sqrt{\frac{K_{ms}}{M_{ms}}}} = \frac{2\pi M_{ms}}{Q_{ms}} \quad (7)$$

where Q_{ms} is the mechanical Q-factor of the driver in free air, which could be determined by the IMP curves obtained by Soundcheck tests of microspeakers. In practice, the microspeaker is promised to have a smaller F_0 while maintaining a higher R_{ms} , thereby effectively reducing the THD%. Therefore, the key to increasing the ratio R_{ms}/F_0 is reducing Q_{ms} . And as a dimensionless number, Q_{ms} is an important parameter characterizing the acoustic performance of the microspeaker. As shown in Figures 13 and 14, the R_E , F_0 , and Z_{max} are obtained by the IMP curve, and Z_E could be calculated as

$$Z_E = r_1 R_E = \sqrt{r_0} R_E = \sqrt{\frac{Z_{max}}{R_E}} R_E = \sqrt{Z_{max} R_E} \quad (8)$$

where R_E is the DC resistance of the microspeaker voice coils, F_0 is the resonance frequency, and Z_{max} is the maximum electrical impedance. Q_{ms} is calculated by Z_E , in which a horizontal line with a y -coordinate of Z_E in the IMP curve intersects the IMP curve at two points, f_1 and f_2 (from left to right); we have [22,53]

$$Q_{ms} = \frac{F_0}{f_2 - f_1} \quad (9)$$

where f_1 and f_2 correspond to the lower frequency at Z_E and the higher frequency at Z_E , respectively. According to Equations (8) and (9), the Q_{ms} of all samples could be calculated, as shown in Figures 13 and 14.

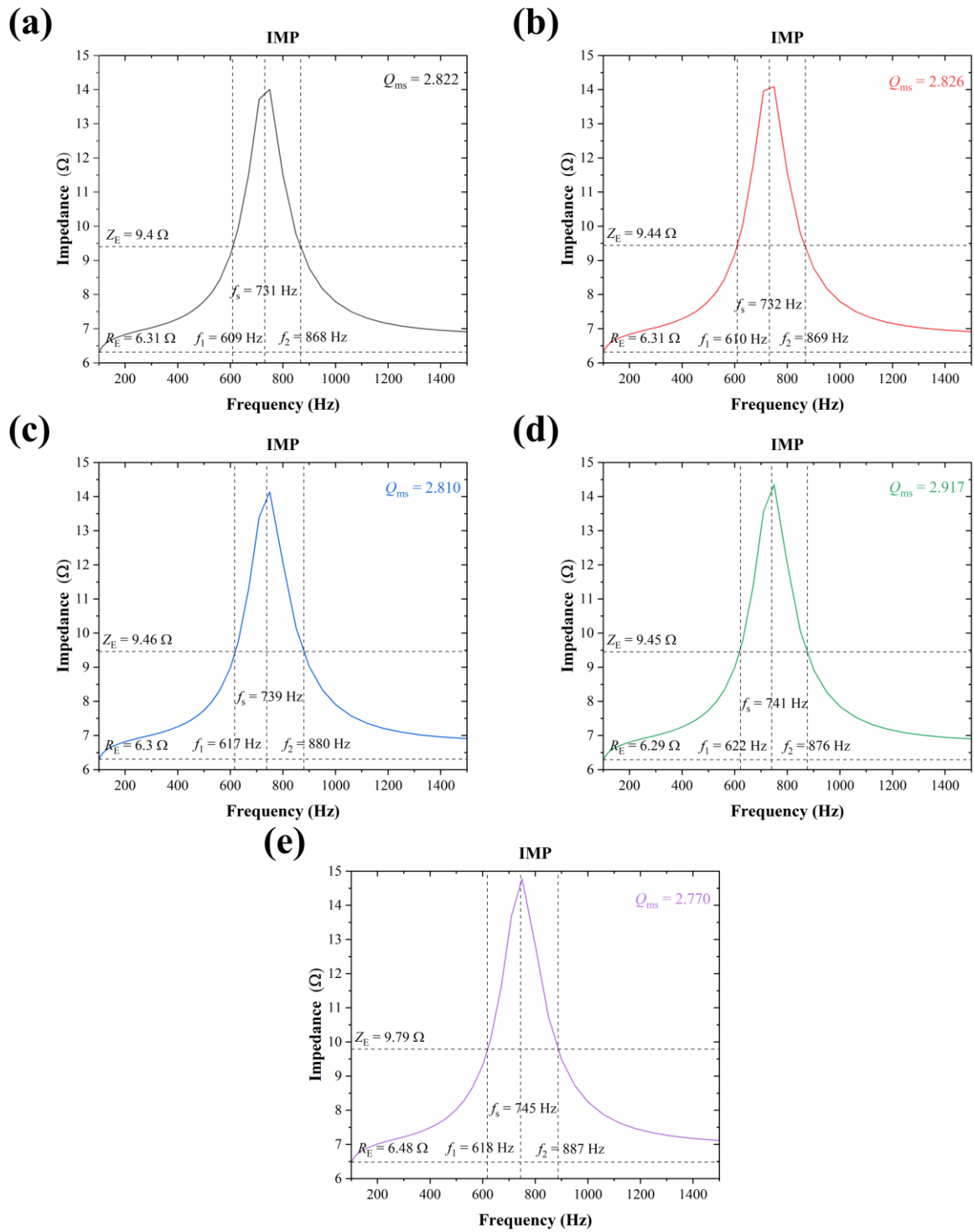


Figure 13. IMP curves of samples in the low-F range and parameters used to calculate Q_{ms} : (a) AEM-90-1; (b) AEM-90-2; (c) AEM-90-3; (d) AEM-90-4; (e) AEM-90-5.

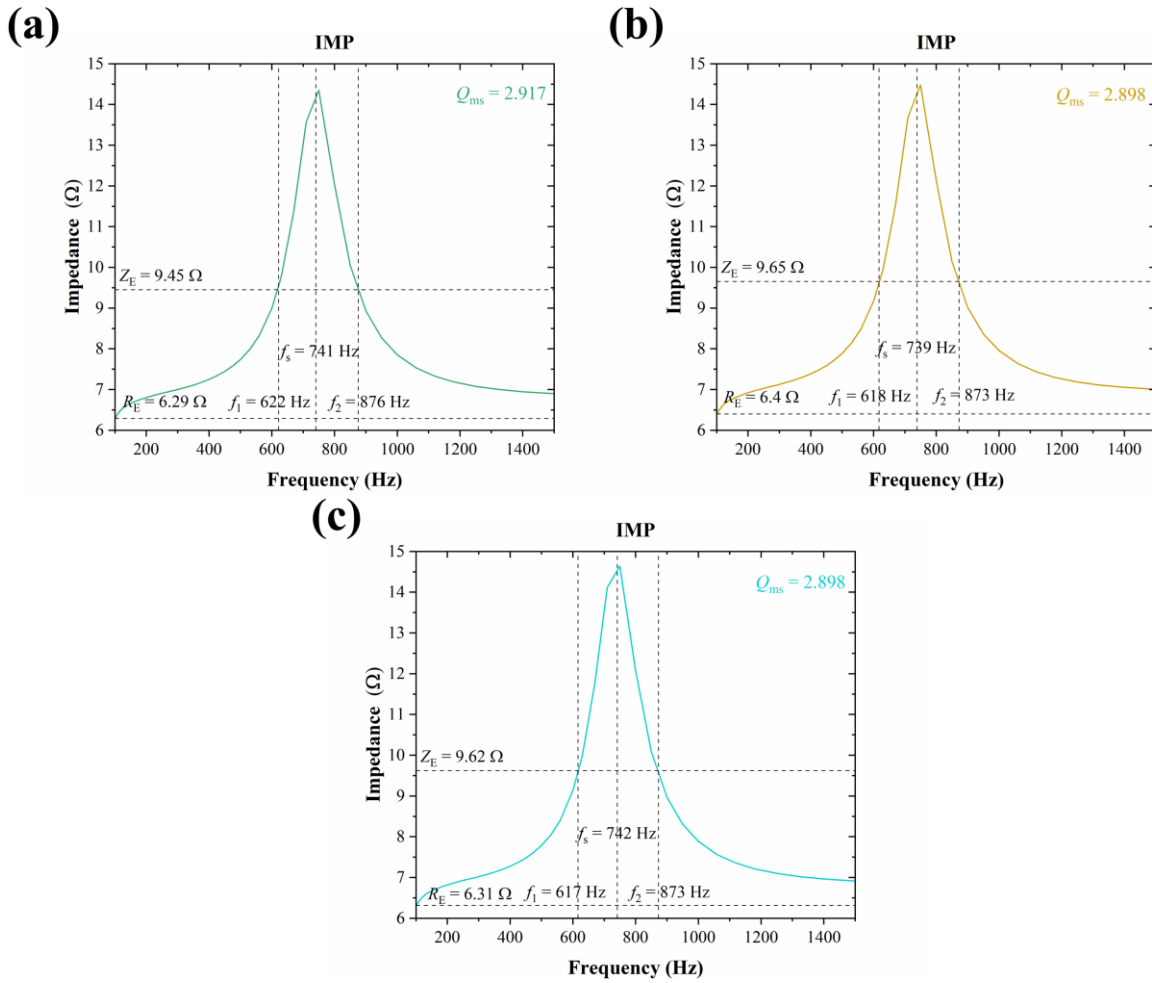


Figure 14. IMP curves of samples in the low-F range and parameters used to calculate Q_{ms} : **(a)** AEM-90-4; **(b)** AEM-80-4; **(c)** AEM-100-4.

Figure 13 shows the IMP curves of samples with different compositions in the low-F range and parameters used to calculate Q_{ms} , and **Figure 14** shows other samples with different thicknesses. Considering the actual applications, microspeakers with relatively low F_0 and relatively high R_{ms} are preferred since the THD% could keep in a low value and the sound quality could be guaranteed. Thus, the ratio R_{ms}/F_0 should be increased. According to Equation (7), increasing M_{ms} or reducing Q_{ms} could increase that ratio. Considering that the M_{ms} is influenced by the mass of the whole structure of the microspeaker and is not trivial to be tailored, the crucial factor is reducing Q_{ms} . Therefore, from this perspective, although for different application requirements, a lower F_0 is not necessarily better, a larger value of R_{ms}/F_0 is more favorable for the tuning of the diaphragm's comprehensive acoustic performance. Hence, AEM-90-5 has the best overall performance.

3.6. Applications and potential limitations

Up to now, the microspeakers with structures illustrated in **Figure 11**, fabricated by “AEM-90-5” diaphragms, have been put into mass production. Nevertheless, the diaphragm material still needs to be updated continuously according to the iterations of cellphone products, especially for flagship products entailing large amplitude and

high damping performance. Some potential limitations of using AEM diaphragms in commercial applications are discussed below.

- 1) Due to the fact that the T_g of AEM (usually $-30\text{ }^{\circ}\text{C}\sim-20\text{ }^{\circ}\text{C}$) is relatively high in synthetic rubber, the AEM diaphragms used in different seasons (particularly in winter and summer) exhibit different E , resulting in fluctuations in F_0 of microspeakers. However, usually a proper range of F_0 of the product is accepted, except for a few products with F_0 exceeding the upper limit of the specifications.
- 2) Given that the injection molding equipment and techniques are established without consideration of cost, the liquid silicone rubber (LSR) could be an appropriate substitute for AEM in terms of waterproof performance. This is due to the fact that the AEM diaphragm should be combined with other components to achieve the same performance.
- 3) Other diaphragm materials, like hydrogenated nitrile rubber (HNBR), which have not been fully investigated, could be the potential substitutes of AEM. Then, the thickness restrictions of the diaphragm could be loosened from $\geq 60\text{ }\mu\text{m}$.

4. Conclusions

Rubber diaphragms are the development trend of the new generation of diaphragm materials for microspeakers. In this paper, the well-performed moving-coil microspeakers based on rubber diaphragms were fabricated by solvent casting, thermoforming, and assembling processes. The relatively low F_0 (745 Hz), THD% (THD265 = 39.82%), and Q_{ms} (2.770), and relatively high SPL (FR2000 = 94.77 dB), electrical impedance (IMP2000 = 7.04 Ω), R_{ms} (0.134 kg/s), and X_{max} (0.58 mm) are achieved. Compared to traditional PEEK, TPEE, and other polymer-based microspeakers, our products have a large amplitude, with no obvious plastic deformation occurring at X_{max} , and excellent sound quality with low distortion.

At the same time, by analyzing the mechanical and acoustic properties of each sample, the pattern of F_0 increasing with E and F_0 increasing with R_{ms} is obtained. The actual changing rule of R_{ms} and F_0 is complex and is related to the vibration mass of the microspeaker, the arrangement of the voice coil, the performance of the dome, and the quality of the damping adhesives, etc. There are few reports in the literature, and some reports are based on derivations from simulation results, which still have a certain deviation from reality. This paper calculates K_{ms} and Q_{ms} through finite element simulation with quasi-static loading of the vibration system and IMP curves, confirming the changing rule of R_{ms} , F_0 , and E , and reaches the conclusion that the microspeaker assembled by diaphragm AEM-90-5 has the best overall performance.

Conflict of interest: The author declares no conflict of interest.

Nomenclature

X_{max}	Maximum excursion of voice coil
F_0	Resonance frequency
R_{ms}	Mechanical resistance of total-driver losses
K_{ms}	Mechanical stiffness of driver suspension

C_{ms}	Mechanical compliance of driver suspension
M_{ms}	Imported mechanical mass of driver diaphragm assembly
Q_{ms}	Mechanical quality factor of driver
Q_{ts}	Total quality factor
T_g	Glass transition temperature
f_s	Resonance frequency of the speaker driver in free space
E	Elastic modulus in the linear elastic range
TS	Tensile strength
$EAB\%$	Elongation at break
FR	Frequency response
IMP	Electrical impedance
THD	Total harmonic distortion
SPL	Sound pressure level
PEEK	Poly ether ketone
TPEE	Thermoplastic polyester elastomer
AEM	Ethyl acrylate rubber

References

1. Thomas S, Visakh PM. Handbook of Engineering and Specialty Thermoplastics: Polyethers and Polyesters. John Wiley & Sons; 2011.
2. Wang CN, Chang JR, Chang WC. Influences of diaphragm materials on the performance of a microspeaker. Journal of Mechanics. 2015; 31(3): 331–336.
3. Bae HJ, Lee HJ, Park K. Ultrasonic assisted thermoforming for rapid fabrication of a microspeaker diaphragm. Microsystem Technologies. 2017; 23: 1677–1686.
4. Huang S, Yang Y, Liu S, Chu X. A large-diaphragm piezoelectric panel loudspeaker and its acoustic frequency response simulation method. Applied Acoustics. 2017; 125: 176–183.
5. Lin M, Trubianov M, Yang K, et al. Lightweight acoustic hyperbolic paraboloid diaphragms with graphene through self-assembly nanoarchitectonics. Science and Technology of Advanced Materials. 2024; 25(1): 2421757.
6. Bi H, Wei Y, Zhou Y, et al. Broadband response diaphragm materials for human acoustics engineering. Small. 2025; 21(1): 2406559.
7. Thiele AN. Loudspeakers in vented box: Part 1. Journal of The Audio Engineering Society. 1961; 22: 181–191.
8. Thiele AN. Loudspeakers in vented box: Part 2. Journal of The Audio Engineering Society. 1961; 22: 192–204.
9. Small RH. Vented-box loudspeaker systems part 1: Small-signal analysis. Journal of the Audio Engineering Society. 1973; 21: 363–372.
10. Small RH. Vented-box loudspeaker systems part 2: Small-signal analysis. Journal of the Audio Engineering Society. 1973; 21: 438–444.
11. Small RH. Vented-box loudspeaker systems part 3: Small-signal analysis. Journal of the Audio Engineering Society. 1973; 21: 549–554.
12. Small RH. Vented-box loudspeaker systems part 4: Small-signal analysis. Journal of the Audio Engineering Society. 1973; 21: 635–639.
13. Hwang, SF, Liu HK, Liao WC, Cheng YK. Fabrication and characterization of diaphragm headphones based on graphene nanocomposites. Materials. 2024; 17(4): 933.
14. Sun Q, Cui C, Li J, et al. Microstructure, mechanical properties, and adhesion behavior of DLC/W coating on Al-Mg loudspeaker diaphragm for enhancing its acoustic performance. Colloid and Interface Science Communications. 2024; 59: 100778.
15. Jiang, ZX, Park JH, Xu DP, Hwang SM. Analysis and prediction of mid-high peak frequency for microspeaker with side-firing front chamber. Applied Sciences. 2023; 13(2): 1018.

16. Park J, Han J. A study on sound radiation characteristics of slim speaker system. *IEEE Access*. 2023; 11: 63167–63175.
17. Ma Y, Lu Y, Deng N, et al. A PZT MEMS loudspeaker with a quasi-closed diaphragm. *Sensors and Actuators A: Physical*. 2023; 358: 114454.
18. Lee, Y, Choi H, Jang J. Fabrication and characterization of lead lanthanum zirconate titanate ceramic-based fully transparent piezoelectric loudspeakers for next-generation electronic devices. *Sensors and Actuators A: Physical*. 2025; 382: 116087.
19. Xu D, Yu Q, Shen F, et al. An analytical model for a pneumatic vibration isolator with the stiffness effect of the elastomeric diaphragm. *Shock and Vibration*. 2018; 2018(1): 8209290.
20. Lucas I, del Real RP, Michelena MD, et al. Resonance frequency dependence on out-of-plane forces for square silicon membranes: Applications to a MEMS gradiometer. *Sensors and Actuators A*. 2010; 163: 75–81.
21. Kim HJ, Yang WS, No K. Improvement of low-frequency characteristics of piezoelectric speakers based on acoustic diaphragms. *IEEE Transactions on Ultrasonics, Ferroelectrics, and Frequency Control*. 2012; 59(9): 2027–2035.
22. Oh SJ. Relationship between the resonance frequency and Q_{TS} for microspeaker (Korean). *Korean Journal of Materials Research*. 2011; 21(7): 403–409.
23. Oh SJ. Study of the properties of a micro-speaker as functions of the diaphragm thickness (Korean). *Sae Mulli (The Korean Physical Society)*. 2006; 52(6): 536–541.
24. Oh SJ, Kim HY. Correlation between tensile strength of diaphragm and resonance frequency for micro-speaker (Korean). *The Journal of the Acoustical Society of Korea*. 2009; 28(4): 299–307.
25. Yang H, Yao X, Yan H, et al. Anisotropic hyper-viscoelastic behaviors of fabric reinforced rubber composites. *Composite Structures*. 2018; 187: 116–121.
26. Dong Y, Yao X, Xu X. Cross section shape optimization design of fabric rubber seal. *Composite Structures*. 2020; 256: 113047.
27. Han R, Wu Y, Quan X, Niu K. Effects of crosslinking densities on mechanical properties of nitrile rubber composites in thermal oxidative aging environment. *Journal of Applied Polymer Science*. 2020; 137(36): e49076.
28. Han R, Shao Y, Quan X, Niu K. Effects of titanate on the bonding properties of silicone rubber and polyester fabric. *Polymer Composites*. 2021; 42: 2370–2379.
29. Sahoo BP, Naskar K, Dubey KA, et al. Study of dielectric relaxation behavior of electron beam-cured conductive carbon black-filled ethylene acrylic elastomer. *Journal of Materials Science*. 2013; 48: 702–713.
30. Xin H, Shepherd DET, Dearn KD. Strength of poly-ether-ether-ketone: Effects of sterilisation and thermal ageing. *Polymer Testing*. 2013; 32: 1001–1005.
31. Lilaonitkul A, Cooper SL. Properties of polyether-polyester thermoplastic elastomers. *Rubber Chemistry and Technology*. 1977; 50(1): 1–23.
32. Medalia AI. Elastic modulus of vulcanizates as related to carbon black structure. *Rubber Chemistry and Technology*. 1973; 46(4): 877–896.
33. Schön P, Dutta S, Shirazi M, et al. Quantitative mapping of surface elastic moduli in silica-reinforced rubbers and rubber blends across the length scales by AFM. *Journal of Materials Science*. 2011; 46: 3507–3516.
34. Jiang ZX, Park KH, Hwang SM. Design and analysis of watch speaker to enhance waterproof performance by using liquid silicone rubber side diaphragm. *Sensors & Actuators A: Physical*. 2022; 338: 113452.
35. Kim KM, Park K. Numerical investigation on vibration characteristics of a micro-speaker diaphragm considering thermoforming effects. *Journal of Mechanical Science and Technology*. 2013; 27(10): 2923–2928.
36. Klippel GmbH. Klippel product brochure. Available online: http://www.klippel.de/uploads/media/KLIPPEL_Brochure_RnD_QC_CTR.pdf (accessed on 1 February 2024).
37. Wu YT, McBride E. Ethylene-acrylic elastomers. In: Kirk RE, Othmer DF (editors). *Kirk–Othmer Encyclopedia of Chemical Technology*. John Wiley & Sons; 2000. pp. 696–703.
38. Kumar ES, Das CK, Banik K, Mennig G. Viscoelastic properties of in situ composite based on ethylene acrylic elastomer (AEM) and liquid crystalline polymer (LCP) blend. *Composites Science and Technology*. 2006; 67: 1202–1209.
39. Gao T, Na B, Choi H, Chung K. Effect of zinc oxide induced metal-ligand crosslink on the mechanical properties in the ethylene acrylic elastomer (AEM). *Materials Letters*. 2018; 214: 154–157.
40. Campos PV, Albuquerque ARL, Angélica RS, Paz SPA. FTIR spectral signatures of amazon inorganic phosphates: Igneous, weathering, and biogenetic origin. *Spectrochimica Acta Part A: Molecular and Biomolecular Spectroscopy*. 2021; 251: 119476.

41. Eisa MY, Al Dabbas M, Abdulla FH. Quantitative identification of phosphate using X-Ray diffraction and Fourier transform infrared (FTIR) spectroscopy. *International Journal of Current Microbiology and Applied Sciences*. 2015; 4(1): 270–283.
42. Osswald J, Fehr KT. FTIR spectroscopic study on liquid silica solutions and nanoscale particle size determination. *Journal of materials science*. 2006; 41: 1335–1339.
43. Ellerbrock R, Stein M, Schaller J. Comparing amorphous silica, short-range-ordered silicates and silicic acid species by FTIR. *Scientific Reports*. 2022; 12: 11708.
44. Klippel W. Prediction of speaker performance at high amplitudes. Available online: http://www.klippel.de/fileadmin/klippel/Files/Know_How/Literature/Papers/Prediction_of_speaker_performance_at_high_amplitudes_01.pdf (accessed on 1 February 2024).
45. Klippel W, Schlechter J. Distributed mechanical parameters describing vibration and sound radiation of loudspeaker drive units. Available online: https://www.klippel.de/fileadmin/klippel/Files/Know_How/Literature/Papers/Distributed%20parameter.pdf (accessed on 1 February 2024).
46. Dong G. Sound quality improvement of dynamic loudspeaker by material selection of diaphragm. In: *Proceedings of the 2022 International Conference on Acoustics, Fluid Mechanics and Engineering and the 12th Green's Function Seminar (AFME&GFS 2022)*; 25–27 November 2022; Nanjing, China.
47. Lin JM, Lin CH. A novel flexible planar loudspeaker with coils on polyimide diaphragm. *Journal of Vibroengineering*. 2017; 20(1): 774–781.
48. Lee K, Seo J, Kwon SS, et al. Vibroacoustic characteristics of a specific patterned polymer with graphene for an electrostatic speaker. *ACS Applied Materials & Interfaces*. 2023; 15: 7319–7328.
49. Heydt R, Kornbluh R, Eckerle J, Pelrine R. Sound radiation properties of dielectric elastomer electroactive polymer loudspeakers. In: *Proceedings of the Smart Structures and Materials 2006: Electroactive Polymer Actuators and Devices (EAPAD)*; 27 February–3 March 2006; San Diego, CA, USA.
50. Huang J, Feng X, Chen S, Shen Y. Analysis of total harmonic distortion of miniature loudspeakers used in mobile phones considering nonlinear acoustic damping. *The Journal of the Acoustical Society of America*. 2021; 149(3): 1579–1588.
51. Chang C, Wang C, Shiah YC, Huang JH. Numerical and experimental analysis of harmonic distortion in a moving-coil loudspeaker. *Communications in Nonlinear Science and Numerical Simulation*. 2013; 18(7): 1902–1915.
52. Shmilovitz D. On the definition of total harmonic distortion and its effect on measurement interpretation. *IEEE Transactions on Power Delivery*. 2005; 20(1): 526–528.
53. Knapp G. Characterization and optimization of polymer membranes for acoustic applications [PhD thesis]. University of Leoben; 2015.